DOI: 10.1002/chem.200700883

A Polyoxyethylene-Substituted Bimetallic Europium Helicate for Luminescent Staining of Living Cells

Anne-Sophie Chauvin,* Steve Comby, Bo Song, Caroline D. B. Vandevyver,* Frédéric Thomas, and Jean-Claude G. Bünzli*[a]

Abstract: The homoditopic ligand H_2L^{C3} has been designed to form neutral triple-stranded bimetallic helicates of overall composition $[Ln_2(L^{C3})_3]$. The grafting of the polyoxyethylene fragments ensures water solubility and also favors cell penetration while being amenable to further derivatization. The ligand pK_a values have been determined by spectrophotometric titration and range from 3.5 (sum of the first two) to 10.3. The thermodynamic stability of the helicates is large at physiological pH ($\log\beta_{23}$ in the range 22–23). The ligand triplet state has an adequate energy (0–phonon transition at $\approx 20800\ cm^{-1}$) for sensitizing the luminescence of Eu^{III} ($Q = 11\%$). Analysis of the Eu^{III} emission spectrum points to an overall pseudo D_3 symmetry for the metal environment. No significant effect of $[Eu_2(L^{C3})_3]$ is observed on the viability of several cancerous cell lines (MCF-7, HeLa, Jurkat, and 5D10). The cell imaging properties of the Eu^{III} helicate are demonstrated for the HeLa cell line by luminescence microscopy. Bright Eu^{III} emission is seen for helicate concentration $> 50\ \mu M$ and after 20–30 min loading time. The helicate stains the cytoplasm and the permeation mechanism is likely to be endocytosis.

Keywords: bimetallic compounds · helicates · luminescence

Introduction

Chemical tools are essential for the study of in-cellular phenomena and for biomolecular imaging and sensing.[1,2] In this perspective, the versatile luminescent properties of trivalent lanthanide ions are presently the subject of a renewed interest.[3–8] Indeed the sharp, characteristic emission lines of the Ln^{III} ions, which extend from UV to visible and near infrared, are easily recognizable. In addition, the lifetimes of the corresponding excited states are in the micro- or millisecond range, so that time-resolved measurements are feasible with unsophisticated instrumentation, which allows one to eliminate autofluorescence of the biological materials and/or to reach high signal-to-noise ratios. To our knowledge, the first experiments dealing with the staining of biological cells with lanthanide complexes date back to 1969 when Scaff et al. treated bacterial smears (*E. coli* cell walls) with aqueous ethanolic solutions of europium thenoyltrifluoroacetonate and observed the red emission of Eu^{III} in continuous mode and under mercury lamp excitation.[9] The usefulness of lanthanide probes for eliminating the autofluorescence background by time-resolved detection was demonstrated with a Tb^{III} conjugate, formed from a diethylenetriaminepentaacetate (dtpa) chelate sequentially reacted with 4-aminosalicylate and dioleoylphosphatidylethanolamine; this probe has been used successfully as a membrane-staining agent for morphological studies of 3T3 cultured cells.[10] Brightly luminescent Tb^{III} macrocyclic chelates have then been proposed by Bornhop and co-workers as tissue-selective markers.[11–13] Presently, novel highly luminescent Eu^{III} complexes are being tested for cell imaging,[14–16] and in-cellular determination of analytes.[17,18] Increasing the number of detectable probes on a single sample, for instance by designing stains with tunable emission wavelengths and simultaneously tunable excited-state lifetimes, is potentially appealing. In this context, bimetallic functional molecular edifices[19] or peptide-linked lanthanide tags[1] may therefore combine two luminescent, two magnetic, or one magnetic and one luminescent centers in a single dual probe.

[a] Dr. A.-S. Chauvin, S. Comby, Dr. B. Song, Dr. C. D. B. Vandevyver, F. Thomas, Prof. Dr. J.-C. G. Bünzli
Laboratory of Lanthanide Supramolecular Chemistry
École Polytechnique Fédérale de Lausanne (EPFL)
LCSL-BCH 1401 (Switzerland)
Fax: (+41) 21-693-9825
E-mail: anne-sophie.chauvin@epfl.ch
caroline.vandevyver@epfl.ch
jean-claude.bunzli@epfl.ch

Supporting information for this article is available on the WWW under http://www.chemeurj.org/ or from the author.

The methodology we pursue towards the latter strategy is to self-assemble lanthanides ions into triple-stranded bimetallic helical structures,[20,21] amenable to functionalization and biological coupling. The insertion of metal ions into helicates results in their spectroscopic and magnetic properties not only being fully retained due to the protective wrapping of the ligand strands around the metal ions, but even enhanced and in any case tunable. In addition, the regular arrangement of the metal ions along the same axis may result in unusual properties such as directional energy transfer.[22]

During the past years, our laboratory has concentrated on the building up of a library of hexadentate ditopic ligands with bis(benzimidazole)pyridine cores. This molecular design is tailored to induce nine-coordinate, tricapped trigonal prismatic environments around the 4f ions similar to the one found in aqua ions. One series of these potential hosts are unsymmetrical and feature two slightly different tridentate coordinating units. They are therefore tailored for the simultaneous recognition of a heteropair of lanthanide ions,[23–25] with the aim of developing hetero dual probes. For the time being, this approach is, however, limited to organic solvents. The other series of building blocks are symmetrical and bear two carboxylic acid functions. A first example is ligand H_2L^C (Scheme 1) which self-assembles in water to

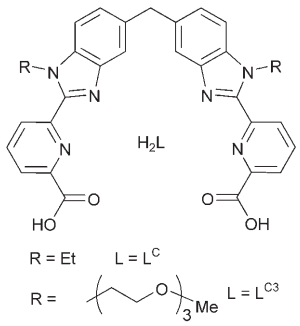

Scheme 1. Symmetrical ditopic ligands for self-assembling bimetallic lanthanide helicates in water.

yield very stable neutral homobimetallic $[Ln_2(L^C)_3]$ helicates. It is noteworthy that the Gibbs free energy associated with the formation of these structures is able to overcome the large hydration enthalpy of the lanthanide ions ($\Delta H^o_{hydr} \approx -3300$ to $-3750\ kJ\,mol^{-1}$). Additionally, the metal ions are very well shielded from water interaction, as demonstrated by the long $Eu(^5D_0)$ lifetime (2.43 ms).[26]

We are now developing a new chemistry for the versatile derivatization of this initial ligand allowing the grafting of solubilizing, chromophoric or coupling groups on either the pyridine or the benzimidazole moieties. We have recently reported a pyridine-derivatized hexadentate ligand forming a Eu^{III} helicate which diffuses into HeLa cells and which stains their cytoplasm.[27] Here we replace the ethyl substituents on the benzimidazole cores of L^C by short polyoxyethylene chains featuring three $-(CH_2)_2O-$ units (H_2L^{C3}, Scheme 1) with the aim of ensuring a better solubility for the resulting helicates, compared with $[Ln_2(L^C)_3]$. The presence of the polyoxyethylene groups should also help avoiding potential stacking of the luminescent tags.[8] We present the adaptable synthetic procedure leading to the isolation of the ditopic receptor, as well as a full thermodynamic and photophysical study of the resulting helicates. Finally, the cytotoxicity of the $[Eu_2(L^{C3})_3]$ helicate towards four different cancerous cell lines is tested, as well as the usefulness of this emissive bimetallic tag for luminescence microscopy of HeLa cells.

Results and Discussion

Ligand synthesis and properties: The main challenge of the chemical synthesis is the sequential introduction of adequate functional groups on the benzimidazole moieties (here the polyoxyethylene chains) and of the carboxylic acid functions in *ortho* position of the pyridines, so that several strategies have been explored with various successes. The polyoxyethylene pendant arms can be grafted either by reacting the brominated derivative with the amine functions of precursor **5**, which beforehand are deprotonated with sodium hydride, or through a Mitsunobu reaction with the alcohol derivative of the arms in presence of azodicarboxylic acid diisopropyl ester (DIAD) and triphenylphosphine. We also tested two oxidative pathways for building the carboxylic acid functions, using various oxidants, starting from either **5c** fitted with methyl alcohol groups or the methylated intermediate **5d**.

The key reaction in the synthesis is the condensation of tetramine **3** (see Scheme 2), obtained upon reduction of the nitro groups of 3,3′-diamino-4,4′-bis(*N*-aminomethyldiphenyl)methane (**2**), with a derivative of picolinic acid functionalized in position 6. The resulting compound must be stable under the harsh conditions provided by the phosphoric acid medium at elevated temperature (210 °C). In addition, depending on the *ortho* substituent on the pyridines of intermediate **5**, further derivatization proved difficult. For instance, condensation of picolinic acid **4a** gave the un-substituted compound **5a** onto which the grafting of two polyoxyethylene pendants was possible, but further attempts to introduce cyano or methyl *ortho* substituents on the pyridine rings were unsuccessful. Other routes starting from **4f** (R = CHO) or **4g** (R = CN) led to the decomposition of the reaction products **5**. Moreover, some of the intermediates **5**, which bear two secondary amines, were far from being soluble in organic or aqueous solvents preventing later modifications; this is exemplified by **5b** obtained either from the carboxamide (**4b**) or ester derivative (**4c**) of picolinic acid. Finally, direct introduction of the methyl alcohol functions in the *ortho* positions of the pyridine rings starting from 6-hydroxymethylpyridine-2-carboxylic acid (**4d**) or from its protected analogue **4e** yielded only traces of the targeted intermediate **5c**.

The final strategy adopted was to start by grafting the polyoxyethylene substituents with the help of a Mitsunobu reaction on intermediate **5d** synthesized from 6-methylpyri-

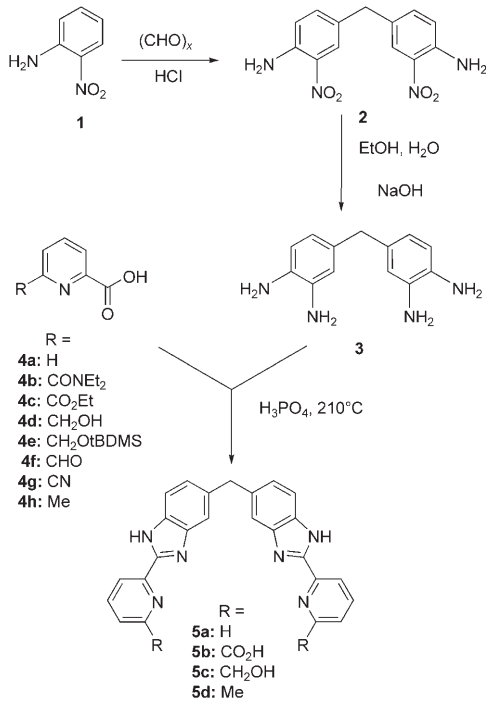

Scheme 2. Synthetic path for the synthesis of key intermediates (**5**).

dine-2-carboxylic acid (**4h**), itself obtained by mono-oxidation of lutidine. Direct oxidation of the resulting intermediate **6** (Scheme 3) proved very difficult and despite many attempts in which the solvent as well as the nature and the amount of oxidant were varied, mono-aldehyde or mono-carboxylic acid derivatives were mainly isolated while larger amounts of oxidant led to decomposition. We therefore decided on a more elaborate three-step route. The first reaction implied activation of the pyridine functions by oxidation with hydrogen peroxide in acetic acid leading to a mixture of di- (**7a**) and tri- (**7b**) *N*-oxide products, the tetra-*N*-oxide form being detected at trace levels only. Secondly, the methyl groups of these products were converted into acetyl functions by addition of acetic anhydride and then transformed into alcohol in methanolic ammonia, which gave better yields than aqueous NaOH. Ultimately, conversion of the alcohol functions into carboxylic acid groups required 30 equivalents of potassium permanganate to ensure optimum conversion, oxidation of the second alcohol function being much more difficult than the first one. Under such experimental conditions partial (5–10%) oxidation of the methylene bridge into a carbonyl moiety occurred, the latter product being separated from H_2L^{C3} by column chromatography followed by preparative HPLC. In summary, the synthesis of the ditopic hexadentate receptor H_2L^{C3} necessitates nine synthetic steps, all of them with a yield up to 60% except the last one, which required extensive purification.

Ligand deprotonation constants were established by spectrophotometric titration of H_2L^{C3} 1.01×10^{-5} M with NaOH at constant ionic strength (0.1 M KCl). The large water solubility of L^{C3} resulting from the polyoxyethylene substituents allowed working in the pH range 0.80–12.88 (Figure S1, Supporting Information), which led to the determination of four of the six pK_a values, as well as the sum of the first two ones. Data were successfully fitted to the following set of Equations (1–5):

$$(H_6L^{C3})^{4+} \rightleftharpoons (H_4L^{C3})^{2+} + 2H^+ \quad (pK_{a1}+pK_{a2}) = 3.5(1) \tag{1}$$

$$(H_4L^{C3})^{2+} \rightleftharpoons (H_3L^{C3})^{+} + H^+ \quad pK_{a3} = 3.2(1) \tag{2}$$

$$(H_3L^{C3})^{+} \rightleftharpoons (H_2L^{C3}) + H^+ \quad pK_{a4} = 4.3(1) \tag{3}$$

$$(H_2L^{C3}) \rightleftharpoons (HL^{C3})^{-} + H^+ \quad pK_{a5} = 7.6(1) \tag{4}$$

$$(HL^{C3})^{-} \rightleftharpoons (L^{C3})^{2-} + H^+ \quad pK_{a6} = 10.3(1) \tag{5}$$

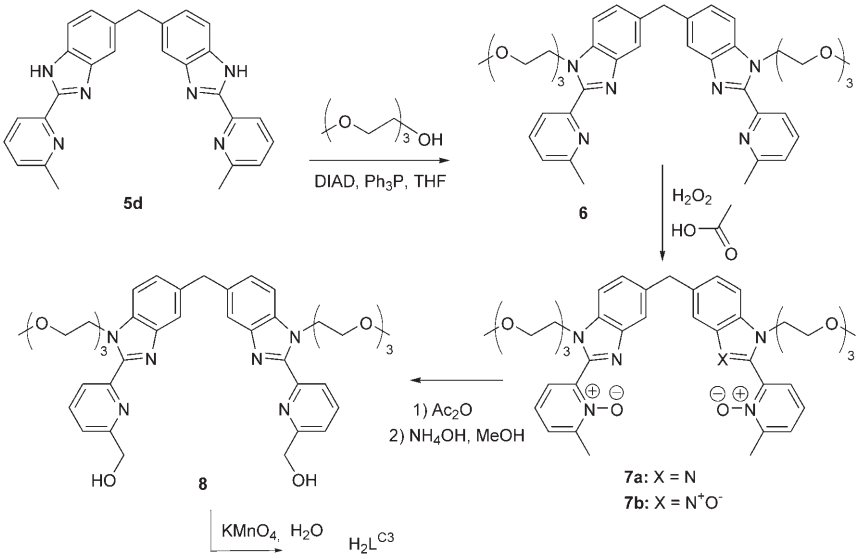

Scheme 3. Synthesis of ligand H_2L^{C3}.

The corresponding distribution diagram is shown in Figure 1. For un-substituted H_2L^{C}, only three protonation constants could be determined because of solubility problems below pH 6;[28] they were assigned on the basis of potentiometric, electronic absorption, fluorescence, as well as ^{1}H and ^{13}C NMR data as follows [the numbering is adapted to Eqs. (1–5) above]: pK_{a6} = 10.1(1) and pK_{a5} = 9.5(2), with a statistical difference of 0.6, correspond to deprotonation of the imidazolyl groups, while pK_{a4} = 6.0(2), and calculated pK_{a3} = 5.4(2) corresponds to the deprotonation of the pyridyl units. Large differ-

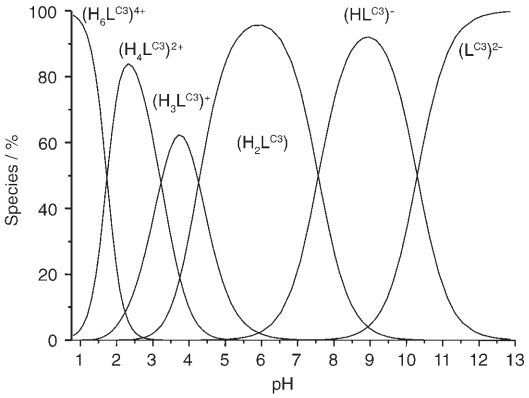

Figure 1. Distribution diagram for H_2L^{C3} 1.01×10^{-5} M versus pH, calculated with the deprotonation constants given in Equations (1–5).

ences with reported pK_a values for benzimidazole, 2-(2′-pyridyl)benzimidazole or 1,10-phenanthroline-2,9-dicarboxylic acid were interpreted in terms of potential hydrogen bonding taking place in the protonated subunits of the ditopic ligand between the pyridinium proton and either the carboxylate or imidazolium groups.[28] In turn, the differences between H_2L^{C} and H_2L^{C3}, $\Delta pK_{a5-3}\approx2$ could be related to less stabilization through hydrogen bonds in view of the larger energy barrier for the *trans–cis* conformational change needed for inducing these bonds, owing to the presence of the bulky polyoxyethylene substituents in H_2L^{C3}.

Formation of the helicates in water: The formation of the $[Ln_2(L^{C3})_3]$ helicates in water is ascertained by electrospray mass spectrometry. Stoichiometric 2:3 solutions of a perchlorate salt (Ln = La, Eu, Gd, Tb, Lu) and of the ligand (3×10^{-4} M in water) were prepared and analyzed in presence of 10% of acetonitrile to induce ionization. In all cases, a peak corresponding to a +2 charged species $\{[Ln_2(L^{C3})_3]+2H\}^{2+}$ was observed. Typical examples are shown on Figure 2 in which the shape of this peak and its isotopic distribution are shown to be in agreement with theoretical simulations. Numerical data for molecular peaks corresponding to the 2:3 helicates for all investigated lanthanides are listed in Table 1. Accuracy of the experimental *m*/*z* measurements is in the range 20–60 ppm which is satisfying taking into account that the average mass accuracy achievable with the spectrometer used is 5 ppm (over the mass range extending from 400–900 Da). No species corresponding to the 1:3 or 2:2 complexes could be evidenced, pointing to the 2:3 helicates being probably the major species in solution.

To quantify the Ln^{III} interaction with H_2L^{C3}, we have performed spectrophotometric titrations of the ligand 10^{-5} M by lanthanide perchlorate solutions 5×10^{-3} M, up to a total concentration ratio $R=[Ln]_t/[H_2L^{C3}]_t=4$. The UV/Vis spectra display a well defined isobestic point at 322 nm (Figure 3, top) and evolving factor analysis usually points to the presence of four absorbing species. Several models were tested, but data were best fitted by non-linear least-squares techniques to the following set of equations (protons and charges are omitted):

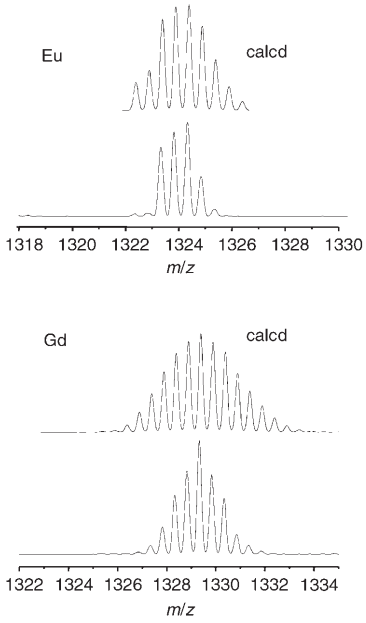

Figure 2. Parts of the electrospray mass spectra of solutions containing 2:3 stoichiometric amounts of Ln^{III} and H_2L^{C3} in water/acetonitrile 90:10, Ln = Eu (top) and Gd (bottom). Calculated spectra are shown above the experimental data; $[H_2L^{C3}]_t=3\times10^{-4}$ M.

Table 1. Mass spectrometric data for H_2L^{C3} and stoichiometric 2:3 solutions ($Ln:H_2L^{C3}$, Ln = La, Eu, Gd, Tb, Lu) in water/acetonitrile 90:10.[a]

	m/*z* (obsd)[b]	*m*/*z* (calcd)	Δ(*m*/*z*) [ppm]	*MW* [Da][c]
H_2L^{C3}	783.3356	783.3354	0.26	783.33
La	1310.3040	1310.3820	60	2618.74
Eu	1324.3270	1324.3949	51	2646.78
Gd	1329.3300	1329.3949	49	2656.78
Tb	1330.3704	1330.4010	23	2658.79
Lu	1346.3691	1346.4164	35	2690.82

[a] The observed and calculated values refer to the most abundant peak. [b] $[M+H]^+$ for H_2L^{C3}, $\{[M+2H]^{2+}\}/2$ for the 2:3 helicates. [c] Molecular weight of the parent species, $C_{123}H_{132}N_{18}O_{30}Ln_2$ for the complexes.

$$3\,L^{C3} + Ln \rightleftharpoons [Ln(L^{C3})_3] \quad \log\beta_{13} \tag{6}$$

$$3\,L^{C3} + 2\,Ln \rightleftharpoons [Ln_2(L^{C3})_3] \quad \log\beta_{23} \tag{7}$$

$$L^{C3} + 2\,Ln \rightleftharpoons [Ln_2(L^{C3})] \quad \log\beta_{21} \tag{8}$$

Residuals were 1.4×10^{-4} (La), 5.7×10^{-4} (Eu), and 3.9×10^{-4} (Lu). Spectra are heavily correlated (Figure S2, Supporting Information) so that the conditional constants collected in Table 2 have to be taken with care. Comparing with the $\log\beta_{23}$ values published for the helicates with H_2L^{C}, the introduction of the polyoxyethylene substituents in H_2L^{C3} is clearly detrimental to the overall stability of the 2:3 complexes. However, the stability of the latter remains large enough to envisage in vitro applications. Indeed, as shown in Figure 3 (bottom) for Eu^{III} and a total concentration of

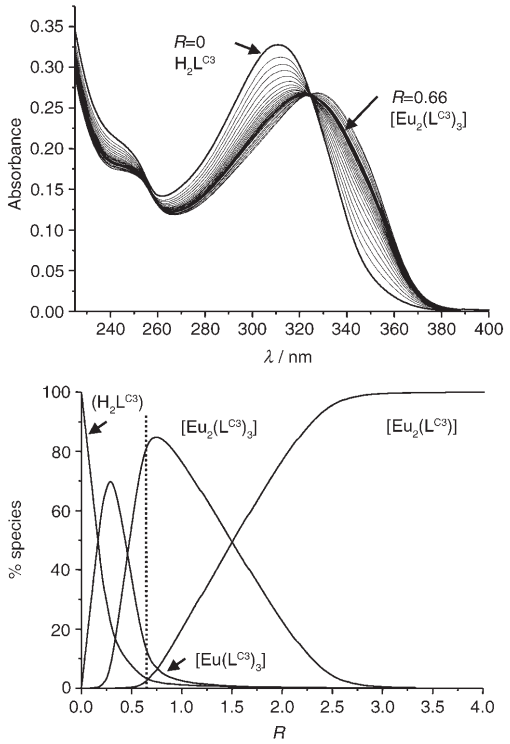

Figure 3. Top: UV/Vis spectra of H_2L^{C3} 10^{-5} M in water at pH 7.4 (Tris-HCl 0.1 M) in presence of increasing amounts of $Eu(ClO_4)_3$ ($R = [Eu]_t/[H_2L^{C3}]_t = 0$–4). Bottom: distribution diagram drawn with the conditional constants reported in Table 2 and for $[H_2L^{C3}]_t = 10^{-4}$ M.

Table 2. Conditional stability constants (pH 7.4, Tris-HCl 0.1 M; 25 °C) for the systems Ln/H_2L^{C3} compared to $\log\beta_{23}$ for Ln/H_2L^{C} (data from ref. [26]).[a]

L	Constant	La	Eu	Lu
L^{C3}	$\log\beta_{13}$	[b]	16.8(1)	17.0[c]
	$\log\beta_{23}$	22.7(2)	23.4(1)	23.1(1)
	$\log\beta_{21}$	10.9(1)	11.4(1)	11.0(1)
L^{C}	$\log\beta_{23}$	30(1)	26.1(4)	27.3(6)

[a] Standard deviations are given within parentheses. [b] For La, a model with three absorbing species gave the best results. [c] Value fixed, otherwise convergence was not reached

10^{-4} M in ligand (i.e., similar to the one used for cell staining experiments), the solution contains only 3% of free ligand and 3% of 2:1 complex, while the helicate is the major species in solution (82%). For a millimolar solution the latter proportion reaches 91% and uncomplexed ligand accounts for less than 0.5%. These findings are consistent with the ESI-MS data reported above.

Ligand-centered photophysical properties: The uncomplexed ligand H_2L^{C3} displays two main absorption bands (Figure S1, Supporting Information) centered at 245 nm and 310–315 nm, depending on pH, and with a shoulder at 330–340 nm; molar absorption coefficients ε for the deprotonated form $(L^{C3})^{2-}$ are 21550 and 31600 $M^{-1}cm^{-1}$, respectively. These bands are essentially generated by $\pi\rightarrow\pi^*$ transitions involving intramolecular electron transfer from benzimidazole to pyridine and carboxylic groups, respectively, according to CAChe calculations. Upon complexation, the main band broadens and sustains a bathochromic shift of about 15 nm, to 326 nm ($\varepsilon = 80000\ M^{-1}cm^{-1}$ for the 2:3 species). Upon excitation into the lowest energy band, emission from the singlet $^1\pi\pi^*$ state is seen as a two-component band with maxima at 376 and 403 nm (Figure 4 and Figure S3, Supporting Information), which sustains a blue shift of about 40 nm upon decreasing the temperature to 77 K. At the latter temperature, time-resolved measurement reveals a broad band with a maximum at 478 nm (0-phonon component at 453 nm) and which extends up to 650 nm, with a vibronic progression of about 1500 cm^{-1} typical of aromatic compounds (ring breathing mode). The emission spectra of the 2:3 complexes with La^{III} and Lu^{III} are very similar, with minor shifts, while the phosphorescence spectrum of the Gd^{III} helicate displays a marked difference in the intensity of the vibronic components.

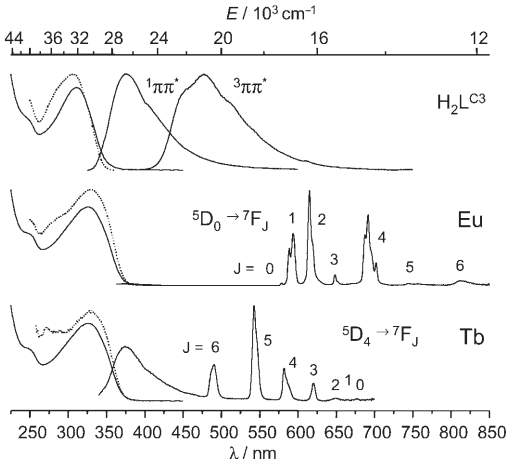

Figure 4. Photophysical properties of H_2L^{C3} and its Ln/H_2L^{C3} 2:3 solutions with Eu^{III} and Tb^{III} at room temperature in Tris-HCl 0.1 M, total ligand concentration 4.5×10^{-5} M. Left: absorption (——) and excitation (•••••) spectra; right: emission spectra ($\lambda_{ex} = 310$–326 nm) recorded without delay, except for $^3\pi\pi^*$ (50 μs delay, 77 K). Vertical scale: arbitrary units; spectra are not drawn to scale.

The triplet state luminescence decay at 77 K is bi-exponential, in line with the presence of two aromatic systems on the ligand. For unbound H_2L^{C3}, the corresponding lifetimes are quite long, 50 ms (15% contribution to the decay) and 430 ms (85%). The long lifetime decreases to approximately 300 ms for the helicate with La^{III} and to 200 ms for the other systems (Ln = Gd, Lu). The shorter lifetime is not much affected in the La^{III} system but decreases to 5 and 17 ms for Gd^{III} and Lu^{III}, respectively. These lifetimes are substantially shorter than those reported previously for H_2L^{C} for which only the longer lifetime could be extracted from the luminescence decays: 776 ± 10 ms, and its helicates with La^{III} (246 ms) and Lu^{III} (181 ms),[26] a fact which we trace back to the presence of the polyoxyethylene substituents which confer more fluxionality to the ligand. At room tempera-

ture, the $^3\pi\pi^*$ emission disappears for the helicates with Eu^{III} and Tb^{III}, and $^1\pi\pi^*$ emission is considerably weakened for Eu^{III}, but not for Tb^{III} (Figure 4). Conversely, a faint residual triplet state emission remains at 77 K while singlet state emission is still sizeable for both helicates (Figures S3, S4, Supporting Information).

Lanthanide-centered photophysical properties: As shown on Figure 4, the Eu^{III} and Tb^{III} helicates mainly display the characteristic metal-centered emission lines from the Eu($^5D_0$) and Tb($^5D_4$) excited states upon ligand excitation. Energy transfer from the ligand is further established by the excitation spectra matching the absorption spectrum of the ligand.

The $[Eu_2(L^{C3})_3]$ emission spectrum may be interpreted as arising from a main species with a single chemical environment displaying pseudo D_3 symmetry: the $^5D_0\rightarrow{}^7F_0$ transition appears as a very symmetrical, faint band (Figure S5, top, Supporting Information) and the $^5D_0\rightarrow{}^7F_J$ transitions display two, two and four main components for $J=1$, 2, and 4, in line with group-theoretical predictions for this symmetry (0, 2, 2, and 4 allowed transitions for $J=0$, 1, 2, and 4).[29] The splitting of the $^7F_1$ level is also in line with a trigonal symmetry: the $^5D_0\rightarrow{}^7F_1$ transition displays a sharp band corresponding to transition to the $^7F_1(A_1)$ ligand-field sub-level and a broader one, terminating on the $^7F_1(E)$ sublevel; the A_1–E separation amounts to 150 cm^{-1}, reflecting a B^2_0 crystal field parameter of about -600 cm^{-1}, using the correlation given by Binnemans et al.[30] Moreover, the broadness of the transition to the E component points to a probable splitting of this sub-level, the extent of which is indicative of the deviation from the idealized symmetry;[31] it can be estimated here to be $\approx$45–50 cm^{-1}. Comparable data for the helicate with H_2L^C were 156 cm^{-1} for the A_1–E separation and 56 cm^{-1} for the splitting of the E level (solid state, 10 k). Therefore, we conclude that the metal ion environments are very similar in the two cases. The only noticeable spectroscopic difference is the intensity of the hypersensitive $^5D_0\rightarrow{}^7F_2$ transition: intensity ratios amount to 0.01, 1.0, 1.45, 0.11, 1.75, 0.06, and 0.23 for $J=0$–6, whereas they were 0.01, 1.0, 0.89, 0.11, and 1.69 ($J=0$–4) for the helicate with H_2L^C. Since the hypersensitive transition contains sizeable contributions from vibronic components,[32] the larger intensity of this transition in the presently reported compound is again understandable in view of the presence of the polyoxyethylene chains. Another argument in favor of a chemical environment similar to the one in the H_2L^C helicate is the energy of the $^5D_0\rightarrow{}^7F_0$ transition, which amounts to 17235 cm^{-1}. Using a known equation[33] and nephelauxetic parameters $\delta_{carb}=-17.2$ cm^{-1} for the carboxylate and $\delta_{bzp}=-15.3$ cm^{-1} for heterocyclic nitrogen atoms,[34] we find $\tilde{\nu}_{calcd}=17231$ cm^{-1}, quite close to the experimental value.

When the luminescence decays are sampled with short time intervals, the functions are bi-exponential reflecting lifetimes for the Eu($^5D_0$) excited level of 2.2 ± 0.1 ms, which is only slightly temperature dependent (2.6 ± 0.1 ms at 77 K) and 0.54 ± 0.05 ms. In D_2O, only one lifetime is evidenced, 4.0 ± 0.1 ms. This clearly points to no water molecule interacting in the first coordination sphere for the main species, $q=0$ calculated using a known phenomenological equation,[35] much as for the helicate with H_2L^C ($\tau=2.43$ and 4.66 ms).[26] Contribution from the long-lived species to the overall luminescence emission amounts to $\approx$90%, in line with the speciation determined by UV/Vis titration. The second lifetime corresponds to a chemical species with a population of $\approx$10% and for which, on average, $q=1.4$.

The Tb^{III} emission spectrum is dominated by the $^5D_4\rightarrow{}^7F_5$ transition and the Tb($^5D_4$) lifetime is quite short at room temperature, 0.39 ± 0.04 ms. Since this lifetime increases considerably when the temperature is lowered, reaching 2.4 ± 0.1 ms at 77 K, the non-radiative de-activation it reflects is not due to coordination of water molecules but, rather, to a back transfer mechanism since the ligand triplet state has an energy very close to the Tb^{III} excited levels. This phenomenon is, however, less pronounced than in the corresponding compound with H_2L^C for which the Tb($^5D_4$) lifetime decreased from 2.10 ms at 100 K to 0.05 ms at 270 K, an effect caused by the slight hypsochromic shift of the ligand energy levels upon functionalization with the polyoxyethylene substituents.

Finally, the quantum yields of the Eu^{III} and Tb^{III} luminescence have been measured upon ligand excitation in Tris-HCl 0.1 M by two different experimental techniques (see Experimental Section): $Q^{Eu}{}_L$ is equal to 11 ± 1% and $Q^{Tb}{}_L$ to 0.34 ± 0.04%, consistent with the back transfer phenomenon evidenced by the temperature dependence of the Tb($^5D_4$) lifetime. The ligand efficiency for the sensitization of the Eu^{III} luminescence, η_{sens}, can be estimated from:[36]

$$Q^{Eu}{}_L = \eta_{sens} \times Q^{Eu}{}_{Eu} = \eta_{sens} \times (\tau_{obs}/\tau_{rad}) \quad (9a)$$

where $Q^{Eu}{}_{Eu}$ is the intrinsic quantum yield (upon direct metal excitation) and τ_{obs} and τ_{rad} are the observed and radiative lifetimes, respectively; the latter is calculated from:

$$1/\tau_{rad} = 14.65 \times (I_{tot}/I_{MD}) \times n^3 \ [s^{-1}] \quad (9b)$$

where I_{tot}/I_{MD} is the ratio of the total emitted intensity to the intensity of the magnetic dipole transition $^5D_0\rightarrow{}^7F_1$. In our case it is equal to 4.69 and $n=1.334$, so that $\tau_{rad}=6.13$ ms, $Q^{Eu}{}_{Eu}=37$% and therefore $\eta_{sens}=30$%.

Some light on the sensitization process is shed by examining the ratios of the integrated total lanthanide luminescence ($J=0$–6 for Eu^{III} or 6–0 for Tb^{III}) to the singlet and triplet state emissions. For the europium helicate, the $^5D_0/^1\pi\pi^*$ ratio decreases from 17.4 at room temperature to 1.4 at 77 K; triplet state emission is only seen at the latter temperature with a $^5D_0/^3\pi\pi^*$ ratio equal to 2.6. This reflects the moderately efficient $^3\pi\pi^*$-to-$^5D_0$ energy transfer ($\eta_{sens}=30$%), in line with an energy difference between the ligand 0-phonon component of the triplet state and the europium emissive state of about 5000 cm^{-1}. For Tb^{III} the gap is much smaller (1500 cm^{-1}) and back transfer occurs so that the overall ligand-to-$^5D_4$ energy transfer is much less important,

as demonstrated by the $^5D_4/^1\pi\pi^*$ ratio which is small, increasing from 0.40 to 2.0 between room temperature and 77 K. Moreover, the energy difference between the 0-phonon lines of the $^1\pi\pi^*$ and $^3\pi\pi^*$ states ($\approx 6800\ cm^{-1}$) is somewhat over the ideal 5000 cm^{-1} gap for an efficient intersystem crossing,[37] consistent with the ratio $^1\pi\pi^*/^3\pi\pi^* = 1.9$ for Eu^{III}, and 2.2 for Tb^{III} at 77 K. In fact, when the temperature is lowered to 77 K, the band envelopes of the ligand emission are noticeably displaced toward the blue with, as a consequence, a dramatic reduction in the $^5D_0/^1\pi\pi^*$ emission ratio. This is due to the overlap integral between the ligand emission spectrum and the Eu^{III} absorption spectrum being reduced. The large decrease in the $^5D_0/^1\pi\pi^*$ ratio concomitant with the bathochromic shift of the $^1\pi\pi^*$ emission may be indicative that some singlet state energy transfer occurs (e.g. to the $^5L_6$ level located on the high energy side of the ligand $^1\pi\pi^*$ emission). In the case of Tb^{III}, a different trend is observed, the $^5D_4/^1\pi\pi^*$ ratio increasing upon lowering the temperature, while the $^5D_4/^3\pi\pi^*$ ratio is comparable to the one observed for Eu^{III}. We trace this back to an increase in the energy gap between the ligand and the metal ion leading to a substantial reduction in the $Tb(^5D_4)$-to-$^3\pi\pi^*$ back transfer. As for Eu^{III}, participation of the $^1\pi\pi^*$ level to the overall energy transfer onto the metal ion is plausible.

Cytotoxicity of the Eu^{III}-containing solutions: The solutions containing the $[Eu_2(L^{C3})_3]$ helicate stain living cells but before describing luminescence imaging experiments, we address two key questions: i) do the cells remain viable in presence of these solutions over the period of examination under the microscope, and ii) does the helicate survive undissociated in the cells? Influence of the Eu^{III}-containing solutions on the proliferation of several malignant cell lines, 5D10 mouse hybridoma, Jurkat human T leukemia, MCF-7 human breast carcinoma and HeLa cervical adenocarcinoma, was determined by means of the WST-1 assay at time intervals between 0.5 and 24 h. Results for the HeLa cell line are shown on Figure 5 (top). No significant differences could be observed in the proliferation of the cells in absence or presence of the helicate, up to 500 μM. This observation is confirmed by the viability of the cells after 24 h incubation at 37 °C with various concentrations of the 2:3 (Ln/H_2L^{C3}) solutions (Figure 5, bottom) and similar results were obtained for the other cell lines, with viabilities usually ≈90 % (Figure S6, Table S2, Supporting Information). In addition, the cellular membrane damage assessed by measuring the lactate dehydrogenase (LDH) leakage 30 min after incubation with the helicate solution is very small for the cell lines tested (see Table 3). All these data show that the Eu species in the solution, particularly the Eu^{III} helicate, can be considered as non-cytotoxic under the experimental conditions used for luminescence cell imaging.

Secondly, the emission spectrum of the $[Eu_2(L^{C3})_3]$ helicate localized in HeLa cells is almost identical with the spectra measured in the aqueous solution at pH 7.4 (Figure S5, Supporting Information). Firstly, a high resolution scan of the $^5D_0 \rightarrow {}^7F_0$ transition reveals a single, symmetric band in both cases with $\tilde{\nu} = 17235\ cm^{-1}$ and a full width at half height of 22 cm^{-1}, confirming once more the presence of a single major species in these solutions. Secondly, the crystal field splitting of the species in water and in the HeLa cells is the same, and the intensity ratios of the $^5D_0 \rightarrow {}^7F_J$ transitions are similar except for a slight reduction in the intensity of the hypersensitive transition. Finally, the lifetimes of the Eu-($^5D_0$) level are comparable to the ones recorded for the aqueous solution: 2.0 ± 0.2 and 0.58 ± 0.06 ms, respectively. The contribution of the species corresponding to the latter lifetime is somewhat larger in the cells (≈15 %), but the smaller emission intensity renders the bi-exponential fit more difficult and the observed increase is in the experimental error. From these results, we conclude that the speciation hardly changes in the cells and, more specifically, that the helicate remains un-dissociated in the HeLa cells under the experimental conditions used.

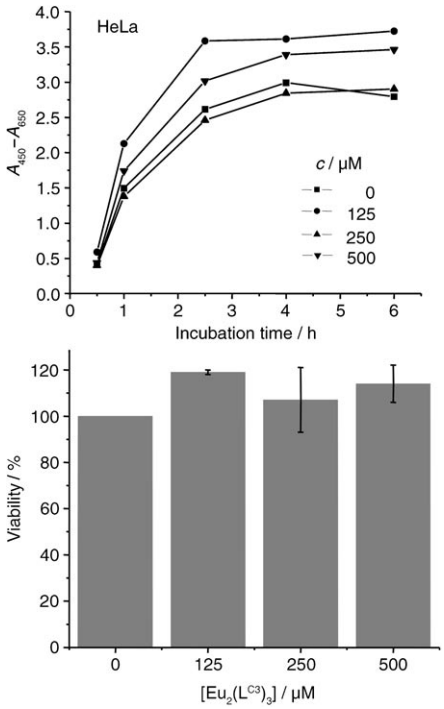

Figure 5. Top: WST-1 proliferation test of HeLa cells in absence or presence of different concentrations of $[Eu_2(L^{C3})_3]$. Bottom: Cell viability values (%), using the same test versus the helicate concentration, after 24 h incubation at 37 °C.

Table 3. Cell cytotoxicity values using the LDH assay at 22 °C and after 30 min incubation of the cells with different concentrations of $[Eu_2(L^{C3})_3]$.

c [μM]	Jurkat	5D10	MCF-7
125	−1.8 ± 0.1	−2.9 ± 1.0	−2.6 ± 0.7
250	−2.2 ± 2.5	−5.9 ± 1.8	−3.7 ± 2.0
500	−0.1 ± 1.8	−1.0 ± 6.9	−2.2 ± 1.9

Luminescence microscopy of HeLa cells: HeLa cells grown on glass bottom cell culture dishes were incubated in cell

culture medium RPMI-1640 containing the Eu^{III} helicate at various concentrations. Cells were examined with a luminescence microscope 7 h after complex loading. The $[Eu_2(L^{C3})_3]$ helicate clearly permeates into the cells and stains their cytoplasm in a concentration-dependent manner (Figure 6 top and S7, Supporting Information). Loading concentrations as low as 50 μM are sufficient to generate reasonably bright images. A counter staining experiment was undertaken in order to confirm the localization of the helicate. Live cells were loaded with the helicate and subsequently with acridine orange, which is a nucleic-acid selective metachromic stain useful for cell cycle determination. Acridine orange is known to permeate into the cell nuclei.[38] The luminescence images of Figure 6 (bottom) clearly confirm the localization of the europium complex in the cytoplasm.

In order to define the mechanism by which the cells take up the europium helicate, the time course and temperature dependence of the complex loading were determined. HeLa cells were incubated with a 500 μM solution of $[Eu_2(L^{C3})_3]$ at 37 °C and examined by luminescence microscopy from 15 min to 6 h after complex loading. The first bright spots in the cytoplasm of the cells can be observed as early as 20–30 min after incubation with the helicate (Figure 7, top, and Figure S8, Supporting Information).

The presence of vesicular structures in the cytoplasm of the cells could support an endocytotic uptake mechanism. It is known that such a mechanism can be blocked at 4 °C. In a separate experiment, the cells were therefore loaded with a 250 μM solution of the $[Eu_2(L^{C3})_3]$ helicate in the cell culture medium at 4 °C for 6 h. No europium luminescence could be observed at 4 °C despite the good viability of the cells at this temperature (Figure 7, bottom and Figure S9, Supporting Information), indicating that the complex is likely to enter the cells by this mechanism.

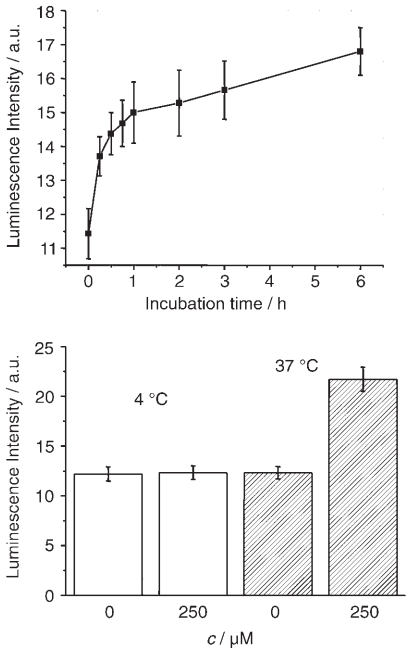

Figure 7. Top: Time dependence of the luminescence intensity of HeLa cells loaded with $[Eu_2(L^{C3})_3]$ 500 μM at 37 °C. Bottom: Comparison of the luminescence intensity from HeLa cells loaded with $[Eu_2(L^{C3})_3]$ 250 μM at 4 and 37 °C.

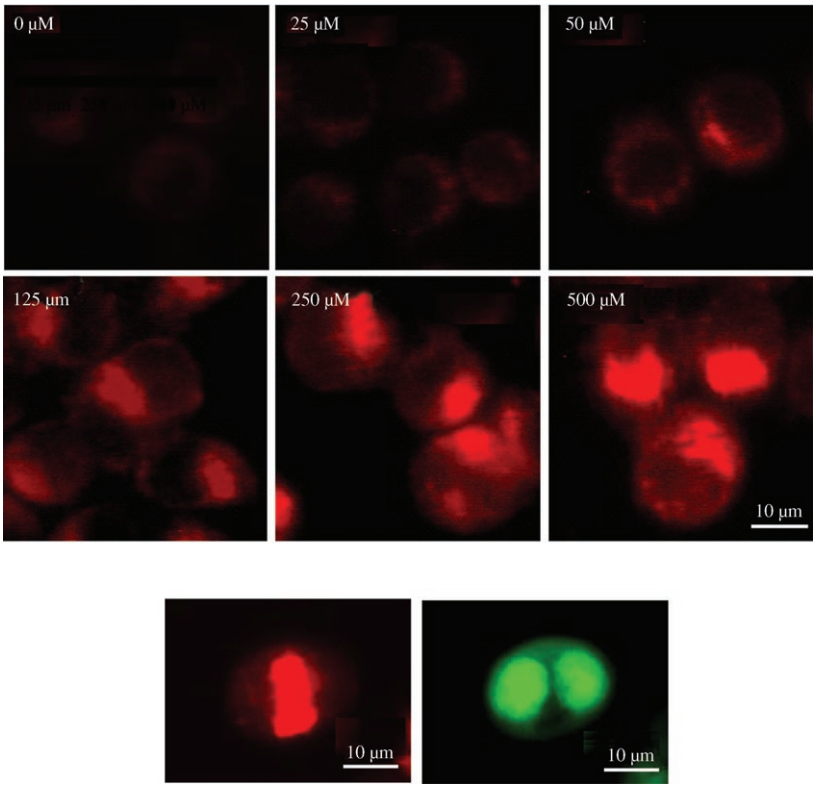

Figure 6. Top: Luminescence images of HeLa cells loaded with different concentrations of $[Eu_2(L^{C3})_3]$ in RPMI-1640 for 7 h at 37 °C (exposure time: 60 s). Bottom: Counter staining experiment with $[Eu_2(L^{C3})_3]$ (red) and acridine orange (AO, green); exposure time: 1 s for Eu and 15 ms for AO.

Conclusion

In this paper, we propose a successful synthetic approach for the derivatization of the benzimidazole moiety of the symmetric, ditopic dicarboxylic ligand H_2L^C to yield H_2L^{C3}. This strategy allows the grafting of polyoxyethylene fragments which are amenable to further derivatization, for instance, for tumor-targeting purposes. We also demonstrate that the resulting triple stranded helicates

$[Ln_2(L^{C3})_3]$ are the main species in solutions with total ligand concentration 10^{-4} M. In addition, the Eu^{III}-containing 2:3 stoichiometric solution possesses the required characteristics for its potential use as a luminescent marker for biological analyses and imaging. It is non-cytotoxic towards several cancerous cell lines, the thermodynamic stability of the main helicate species is large enough at physiological pH, and $[Eu_2(L^{C3})_3]$ easily permeates into the cytoplasm of HeLa cells. The helical edifice remains intact in the cells and the required concentration and incubation time are compatible with practical cell-imaging experiments. The presence of other minor species in the solutions used for the latter experiments (≈10%) is not detrimental since free ligand and metal ion are in trace quantities only and since the second species of some importance is the 1:3 complex which also provides a protective chemical environment for the metal ion. For the time being the only drawback of this luminescent staining solution is its relatively short excitation wavelength, 330 nm, that can be extended to 365 nm by choice of a judicious excitation filter. After this proof of principle, experiments are now in progress in our laboratory to extend the excitation wavelength into the visible range by adequate derivatization. We are also planning to stain other cell lines, the use of time-resolved microscopy, and targeting experiments.

Experimental Section

Starting materials and general procedures: Chemicals and solvents were purchased from Fluka. Solvents were purified by a non-hazardous procedure by passing them onto activated alumina columns (Innovative Technology Inc. system).[39] Stock solutions of lanthanides were prepared just before use in freshly boiled, doubly distilled water from the corresponding $Ln(ClO_4)_3{\cdot}xH_2O$ salts (Ln = La, Lu, Gd, Tb, Eu, x = 2.5–4.5). These salts were prepared from their oxides (Rhône-Poulenc, 99.99%) in the usual way.[40] Concentrations of the solutions were determined by complexometric titrations using a standardized Na_2H_2EDTA solution in urotropine buffered medium and with xylenol orange as indicator.[41]

Analytical measurements: NMR spectra were measured at 25°C on Bruker Avance DRX 400 (^{1}H, 400 MHz) and AV 600 (^{13}C, 99.8 MHz) spectrometers. Spectra of organic compounds were recorded in $CDCl_3$ (99.8%, Aldrich), MeOD (99.8%, Aldrich) or $[D_6]$DMSO (99.8 Aldrich) and those of the helicates in D_2O (99.9%, Aldrich); deuterated solvents were used as internal standards and chemical shifts are given with respect to TMS. The ESI-MS spectra of the ligands were obtained on a Finningan SSQ 710C spectrometer using 10^{-5}–10^{-4} M solutions in acetonitrile/H_2O/acetic acid (50:50:1) or MeOH, capillary temperature 200°C and acceleration potential 4.5 keV. The instrument was calibrated using the horse myoglobin standard and the analyses were conducted in positive mode. ESI-QTOf MS spectra of the complexes were measured on a Q-Tof Ultima API mass spectrometer (Micromass, Manchester, UK) equipped with a Z-spray type ESI source. Phosphoric acid was used for the positive ion mass calibration range of 100–2000 m/z. Data were acquired and processed using Masslynx version 4.0. Electrospray conditions were as follows: capillary voltage, 2.3 kV; source temperature, 80°C; cone voltage, 35 V; and source block temperature, 150°C. The ESI nebulization and drying gas was nitrogen. All experiments were performed in positive ion mode. The sample was introduced via a syringe pump operating at 20 μL min^{-1}. Simulation of spectra was achieved with Molecular Weight Calculator 6.42. UV-visible spectra were measured in 0.2 cm quartz Suprasil cuvettes on a Perkin Elmer Lambda 900 spectrometer. Molecular modeling was performed with the CAChe workpackage 7.5 (Fujitsu, 2000–2006). IR spectra were obtained on a Spectrum One Perkin Elmer FT-IR spectrometer equipped with an ATR accessory. FIR spectra were recorded with an IFS 13v FT-IR spectrometer from Bruker equipped with a pyroelectric DTGS detector. Raman spectra were obtained by means of a Spex 1403 spectrometer with RCA photomultiplier and an argon laser Stabilite 2017 from Spectra-Physics. Elemental analyses were performed by Dr. Eder, Microchemical Laboratory of the University of Geneva.

Preparation of ligands (see Schemes 2 and 3): H_2L^C used for comparison purposes was prepared as previously described.[26] The syntheses of **2** and **3** were adapted from the procedure described for 3,3′-dinitro-4,4′-bis(*N*-aminomethyldiphenyl)methane;[42] 6-methyl-pyridine-2-carboxylic acid **4b** was prepared in 60% yield according to Black et al.[43]

3,3′-Dinitro-4,4′-diaminodiphenylmethane (2): Nitro-2-aminobenzene (12.5 g, 9.05 mmol) and *p*-formaldehyde (1.35 g, 4.52 mmol) were heated in 25% HCl (200 mL) for 5 h. The orange-yellow solution was then poured in water (600 mL) and neutralized with 25% aqueous ammonia (pH 10). The precipitate was filtered, washed with water, and dried under vacuum to give a yellow-orange solid (23.4 g, 90%). ^{1}H NMR ($CDCl_3$): δ = 7.93 (s, 1H, H_{ar}), 7.16 (d, 1H, H_{ar}), 6.75 (d, 1H, H_{ar}), 3.81 ppm (s, 1H, -CH_2-); ESI-MS: m/z: calcd for: 289.10; found: 289.53 $[M+H]^+$; elemental analysis calcd (%) for $C_{13}H_{12}N_4O_4{\cdot}1.3H_2O$: C 50.10, H 4.72, N 17.98, found: C 50.13, H 4.46, N 17.93.

3,3′,4,4′-Tetraaminodiphenylmethane (3): Compound **2** (3 g, 10.4 mmol) was mixed with zinc (10.9 g, 166 mmol) and refluxed in ethanol (120 mL) under N_2; 30 mL of aqueous NaOH 0.1 M were then added dropwise under vigorous stirring. After 1 h the orange solution should turn to pale yellow, otherwise additional amounts of NaOH have to be added. After additional 2 h refluxing, the solution was filtered and the filtrate evaporated under reduced pressure. The crude product was poured into water (100 mL), filtrated, rinsed with water until neutral pH and dried under vacuum (2 mbar) at RT. The brownish solid was stored under vacuum and should be used without delay (6 g, 70%). ^{1}H NMR ($[D_6]$DMSO): δ = 6.37 (d, 1H, H_{ar}), 6.77 (s, 1H, H_{ar}), 6.17 (d, 1H, H_{ar}), 3.39 ppm (s, 1H, -CH_2-); ESI-MS: m/z: calcd for: 229.15; found: 229.47 $[M+H]^+$.

Compound 5d: Freshly prepared **3** (1.3 g, 5.6 mmol) was introduced with 6-methylpyridine-2-carboxylic acid (**4b**; 1.6 g, 11.6 mmol) and polyphosphoric acid (20 mL) in a two-neck 50 mL flask equipped with a thermometer and a distillation apparatus. The mixture was heated with a DrySyn apparatus at 180°C, all the water removed by distillation and the temperature then increased to 210°C. After stirring 6 h, the temperature was decreased to approx. 60°C and the viscous brown residue poured into ethanol (150 mL). A green solid formed, which was filtrated, poured in 0.1 M NaOH (100 mL) and the pH was adjusted to 13–14 by addition of 5 M NaOH. The brown solid was filtrated, rinsed with water, and dried at 70°C under vacuum (2 mbar) for 12 h (2 g, 82%). ^{1}H NMR ($[D_6]$DMSO): δ = 8.18 (d, 1H, H_{ar}), 7.77 (dd, 1H, H_{ar}), 7.48 (d, 1H, H_{ar}), 7.43 (s, 1H, H_{ar}), 7.25 (d, 1H, H_{ar}), 7.13 (d, 1H, H_{ar}), 3.17 (s, 1H, -CH_2-), 2.55 ppm (s, 3H, -CH_3); ^{13}C NMR ($[D_6]$DMSO): δ = 158.12, 152.83, 149,59, 140.92, 140.20, 137.70, 136.00, 123.70, 123.32, 118.78, 116.33, 115.45 ppm; elemental analysis calcd (%) for $C_{27}H_{22}N_6{\cdot}1.5NaOH{\cdot}2H_2O$: C 61.59, H 5.59, N 15.96, found: C 61.54, H 5.40, N 16.46; MALDI-TOF-MS: m/z: calcd for $[M]^+$: 430.19; found: 430.19.

Compound 6: Diamine **5d** (2 g, 4.65 mmol) was dissolved in THF (200 mL) in presence of triethyleneglycolmonomethylether (4.6 mL, 29.8 mmol), and triphenylphosphine (7.8 g, 29.8 mmol). Azodicarboxylic acid diisopropyl ester (5.8 g, 29.8 mmol) was added dropwise at room temperature. The orange solution was refluxed for 12 h then the solvent was removed under reduced pressure, and the residue was re-dissolved in dichloromethane (150 mL), washed with aqueous HCl 0.1 M (100 mL) and with water (2×100 mL). The organic phase was dried over Na_2SO_4 and evaporated and the resulting crude solid was purified by column chromatography (silica gel; CH_2Cl_2/MeOH 100 → 97:3) to give the disubstituted product **6** as an orange oil (2 g, 64%). ^{1}H NMR ($CDCl_3$): δ = 8.16 (d, 1H, H_{ar}), 7.68 (m, 2H, H_{ar}), 7.43 (d, 1H, H_{ar}), 7.17 (m, 2H, H_{ar}), 4.93 (dd, 2H, -OCH_2-), 4.28 (d, 1H, -OCH_2-), 3.98 (m, 2H, -CH_2-), 3.54–3.42 (dm, 9H, -OCH_2-), 3.31 (s, 3H, -OCH_3), 2.60 ppm (s, 3H, -CH_3);

^{13}C NMR (600 MHz, $CDCl_3$): δ = 157.30, 150.19, 150.08, 149,99, 149.85, 142.73, 141.08, 137.42, 136.68, 136.18, 135.73, 124.55, 124.17, 124.10, 123.03, 122.99, 121.54, 121.50, 119.67, 110.65, 61.70, 58.99, 58.92, 45.53, 45.39, 42.83, 42.54, 24.40 ppm; ESI-MS: *m*/*z*: calcd for $[M+H]^+$: 723.38; found: 723.38, 362.33 $[M+2H]^{2+}$/2; elemental analysis calcd (%) for $C_{41}H_{50}N_6O_6\cdot H_2O$: C 66.47, H 7.07, N 11.34, found: C 66.16, H 7.33, N 11.78.

Compounds 7a + 7b: Compound **6** (200 mg, 0.28 mmol) was dissolved in acetic acid (10 mL) and hydrogen peroxide 30% (1.6 g) was added dropwise. After refluxing 4 h, an additional amount of H_2O_2 was added (1.6 g, 50 equiv) and the solution was further refluxed for 4 h. The reaction was followed by mass spectrometry, giving a mixture of di- and tri-N-oxide compounds; ESI MS: *m*/*z*: di-*N*-oxide: calcd for $[M+H]^+$: 755.38; 755.32, 378.31 $[M+2H]^{2+}$/2; tri-*N*-oxide: calcd for $[M+H]^+$: 771.37; found: 771.34, 386.19 $[M+2H]^{2+}$/2. The solvent was carefully removed and the crude product was dried under vacuum for 2 d (210 mg). **CAUTION**! *Hydrogen peroxide combined with organic compounds is potentially explosive and should be handled in small quantities and with adequate precautions.*

Compound 8: The crude mixture of products **7a + 7b** was dissolved in acetic anhydride (10 mL) and stirred at 70°C for 12 h; the solvent was removed and the resulting residue was dried under vacuum (2 mbar) for 12 h. The completion of the reaction was monitored by mass spectrometry. ESI: *m*/*z*: calcd for $[M+H]^+$: 839.95; found: 839.39, 420.34 $[M+2H]^{2+}$/2; *N*-oxide derivative: *m*/*z*: calcd for: 420.21; found: 855.27 $[M+H]^+$, 428.37 $[M+2H]^{2+}$/2. This product could not be purified and was directly used in the next step by dissolution in a methanolic solution of 7 N ammonia (20 mL) and stirring for 6 h at RT. The solvent was then removed giving an orange oil (150 mg, overall yield: 71%). ^{1}H NMR ($CDCl_3$): δ = 8.26 (d, 1H, H_{ar}), 7.79 (m, 1H, H_{ar}), 7.71 (d, 1H, H_{ar}), 7.53–7.22 (m, 2H, H_{ar}), 7.21 (d, 1H, H_{ar}), 4.93 (d, 2H, -OCH_2-), 4.27 (s, 1H, -CH_2OH), 3.96 (d, 2H, -OCH_2-), 3.57–3.30 (m, 9H, -CH_2-), 3.32 ppm (s, 3H, -OCH_3); ESI MS: *m*/*z*: calcd for $[M+H]^+$: 755.38; found: 755.32, 378.31 $[M+2H]^{2+}$/2.

H_2L^{C3}: Compound **8** (150 mg, 0.2 mmol) was dissolved in 0.1 M NaOH (50 mL) and $KMnO_4$ (92 mg, 0.59 mmol) was added under vigorous stirring. The solution was heated at 70°C for 12 h, filtrated, and the aqueous basic phase was extracted twice with CH_2Cl_2 (50 mL). The pH of the aqueous phase was decreased to 2 before extraction with CH_2Cl_2 (3× 75 mL). The combined organic phases were dried over Na_2SO_4, evaporated and the resulting crude solid was purified by column chromatography (silica gel; MeCN/25% NH_4OH 100→88:12) followed by preparative HPLC (MeCN/H_2O, TFA 0.09%) to give the final H_2L^{C3} product as a slight orange oil (48 mg, 31%). ^{1}H NMR ($CDCl_3$): δ = 8.67 (d, 1H, H_{ar}), 8.26 (d, 1H, H_{ar}), 8.09 (dd, 1H, H_{ar}), 7.85 (d, 1H, H_{ar}), 7.45 (d, 1H, H_{ar}), 7.27 (d, 1H, H_{ar}), 4.93 (d, 2H, -OCH_2-), 4.27 (s, 1H, -CH_2OH), 4.35 (d, 2H, -OCH_2-), 4.13 (d, 2H, -OCH_2-), 3.65–3.48 (m, 9H, -OCH_2-), 3.69 ppm (s, 3H, -OCH_3); ^{13}C NMR (MeOD): δ = 167.43, 150.15, 149.42, 140.09, 139.21, 137.88, 128.69, 128.60, 127.31, 126.89, 126.80, 119.09, 118.99, 118.68, 113.49, 113.28, 72.8, 71.67, 71.46, 71.388, 71.35, 71.22, 58.99 ppm; ESI MS: *m*/*z*: calcd for $[M+H]^+$: 783.34; found: 783.36, 392.33 $[M+2H]^{2+}$/2; elemental analysis calcd (%) for $C_{41}H_{46}N_6O_{10}\cdot NaCl\cdot H_2O$: C 57.31, H 5.63, N 9.78, found: C 57.24, H 5.72, N 9.48.

Preparation of the helicate solutions: The 2:3 helicates ($C_{123}H_{132}N_{18}O_{30}Ln_2$) were synthesized in situ by mixing three equivalents of H_2L^{C3} with two eqs of $Ln(ClO_4)_3\cdot xH_2O$ (Ln = La, Lu, Gd, Tb, Eu, x = 2.5–4.5) in water. When needed, the pH was adjusted to 7.4 with a Tris-HCl 0.1 M buffer solution. **CAUTION!** *Perchlorate salts combined with organic compounds are potentially explosive and should be handled in small quantities and with adequate precautions.*[44]

Spectrophotometric titrations: Protonation constants of H_2L^{C3} were determined with the help of a J&M diode array spectrometer (Tidas series) connected to an external computer. All titrations were performed in a thermostated (25.0 ± 0.1°C) glass-jacketed vessel at μ = 0.1 M (KCl). In a typical experiment a 1.01×10^{-5} M solution of H_2L^{C3} (50 mL) was titrated with a freshly prepared sodium hydroxide solution at different concentrations (10, 4, 1, 0.1 and 0.01 M). After each addition of base, the pH of the solution was measured by a KCl-saturated electrode and the UV/Vis absorption spectrum was recorded using a 1 cm Hellma optrode immersed in the thermostated titration vessel and connected to the Tidas spectrometer. Measurements were conducted in the pH range 0.80–12.88. Using the same equipment, conditional stability constants were determined by titration of H_2L^{C3} by Ln^{III} (Ln = La, Eu, Lu) at fixed pH 7.4 (0.1 M Tris-HCl buffer). Factor analysis[45] and mathematical treatment of the spectrophotometric data were performed with the Specfit software.[46,47]

Luminescence data: Broad-band excited emission spectra were recorded on a Fluorolog FL-3-22 spectrometer from Horiba-Jobin-Yvon Ltd; quartz cells with optical paths of 0.2 cm were used for room temperature spectra, while 77 K measurements were carried out on samples put into quartz Suprasil capillaries. All spectra are corrected for the instrumental function. Quantum yields of the helicates were determined in aerated water in two ways. Firstly with respect to a known standard, $[Ln(dpa)_3]^{3-}$ (Ln = Eu, Q = 24%, Ln = Tb, Q = 22%).[48] Absorbance of the samples and reference was usually kept near 0.2. Total ligand concentration was 3.75×10^{-5} M and the following equation was used:[49]

$$Q_{abs}^{sample} = \left(\frac{A_{ref}}{A_{sample}}\right) \times \left(\frac{S_{sample}}{S_{ref}}\right) \times Q_{abs}^{ref}$$

where A is the absorbance and S are integrated, corrected emission area. Refractive index correction was not needed, all solutions having the same n_D^{20}. The obtained values were 10.0 ± 1.5% for Eu^{III} and 0.34 ± 0.04% for Tb^{III}. Secondly, the quantum, yields were checked by an absolute method[50] based on a home-modified integrating sphere from Oriel.[51] Solutions of the helicates (1.25×10^{-5} M) were introduced into 3 mm OD quartz capillaries (volume needed: about 40 μL) and the instrumental function of the spectrometer was carefully established before measurements; the results were Q = 11.2 ± 0.5 (Eu^{III}) and 0.33 ± 0.02 (Tb^{III}) in very good agreement with the data obtained by the classical method. All data reported are averages of at least three independent measurements. High-resolution emission spectra and excited state lifetimes were measured on a previously described instrumental set-up.[52] It is noteworthy that lifetime determinations with the FL 3-22 spectrometer always yielded perfectly single exponential decays but when measured on the high resolution instruments (Ln = Eu only), which provides a shorter sampling time interval, the best fits were obtained with a bi-exponential function.

For luminescence measurement of the helicate permeated into HeLa cells, the latter at 90% confluency were loaded with the helicate solution (250 μM in RPMI-1640 culture medium) for 6 h, washed with PBS (phosphate buffer saline) ten times, and then harvested with trypsin. The mixture was centrifuged (3000 rpm, 5 min), and the cell pellet was re-suspended in PBS (0.8 mL).

Cell culture: The mouse hybridoma cell line 5D10, the human T leukemia cell line Jurkat (ATCC TIB152), the human breast adenocarcinoma cell line MCF-7 (ATCC HTB-22), and the human cervical adenocarcinoma cell line HeLa (ATCC CCL-2) were used in this study. Cells were cultivated in 75 cm^2 culture flasks using RPMI-1640 supplemented with 5% fetal calf serum (FCS), 2 mM L-glutamine, 1 mM sodium pyruvate, 1% non-essential amino acids, 1% 4-(2-hydroxyethyl) monosodium salt (HEPES) (all from Gibco Cell Culture, Invitrogen, Basel, Switzerland). Cultures were maintained at 37°C under 5% CO_2 and 95% air atmosphere. The growth medium was changed every other day until the time of use of the cells. Cell density and viability, defined as the ratio of the number of viable cells over the total number of cells, of the cultures were determined by trypan blue staining and a Neubauer improved hemacytometer (Blau Brand, Wertheim, Germany).

WST-1 cell proliferation assay: This assay is dependent on the cellular reduction of WST-1 (4-(3-(4-iodophenyl)-2-(4-nitrophenyl)-2*H*-5-tetrazolio)-1,3-benzene disulfonate (cell proliferation reagent WST-1, Roche, Germany) by the mitochondrial dehydrogenases in viable cells to give a dark red formazan product. The viable cell number per well is directly proportional to the production of red formazan, which can be measured spectrophotometrically.[53,54] Cells were seeded in a 96-well tissue culture microplate at a concentration between 1–5 × 10^5 cells per well in 100 μL

culture medium and incubated overnight at 37 °C and 5 % CO_2. The helicate was dissolved in fresh RPMI-1640 medium at 37 °C, at a concentration of 500 μM. The medium was removed from the cell cultures and 100 μL per well of the helicate was added (final concentrations: 500 μM, 250 μM, and 125 μM); 10 μL of WST-1 reagent was added to each well and the plate was shaken for 1 min on a microtiter plate shaker (450 rpm). The plate was further incubated at 37 °C and 5 % CO_2 and the absorbance of the formazan product was measured at 450 nm with an ELISA reader (Spectra MAX 340, Molecular Devices, Sunnyvale, CA, USA). Cell viability was calculated from the absorbance values as:

$$\text{viability}_{\text{WST}}\ [\%] = \frac{(A_{450}-A_{650})_{\text{exp}}}{(A_{450}-A_{650})_{\text{medium}}} \times 100$$

with $(A_{450}-A_{650})$ being the absorbance difference between 450 nm and 650 nm for the cells that were in contact with the complex ("exp") and medium only. The results are expressed as an average over three nominally identical measurements.

Homogeneous membrane integrity assay: The measurement of the leakage of components, such as lactate dehydrogenase (LDH), from the cytoplasm into the surrounding culture medium is a widely accepted method to estimate the number of non-viable cells. LDH leakage was measured for different cell lines by using the CytoTox 96 non-radioactive cytotoxicity assay kit (Promega Corporation, Madison, WI, USA) in which the LDH released from the cells catalyses the conversion of resazurin into resorufin.[55,56] Cells were seeded in a 96-well tissue culture microplate as for the WST-1 test. After addition of the helicate, the plate was further incubated at 37 °C and 5 % CO_2 for 30 min, removed from the incubator and equilibrated to 22 °C; 50 μL of substrate mix solution was then added before final incubation at 22 °C for 10 min. Fluorescence values (λ_{ex} = 530 nm, λ_{an} = 590 nm) were measured with a microplate fluorimeter SAFIR II, from Tecan Schweiz AG. The results are expressed as an average over 3 nominally identical measurements. Maximum LDH release after cell lysis by 9 vol % Triton X-100 and spontaneously released LDH in cells not in contact with the helicate were also measured. The average fluorescence values of the culture medium background were subtracted from all fluorescence values of experimental wells. Cytotoxicity caused by the complex is calculated as follows:

$$\text{cytotoxicity}_{\text{LDH}}\ [\%] = \frac{I_{\text{exp}}-I_{\text{medium}}}{I_{\text{exp,max}}-I_{\text{medium}}} \times 100$$

where I_{exp}, I_{medium}, and $I_{exp,max}$ are fluorescence values for cells in contact with the helicate, for the spontaneous release of LDH by cells not in contact with the helicate, and for lysed cells, respectively. Results are reported in Table 3.

Live cell imaging: Cells for fluorescence microscopy were seeded on glass bottom cell culture dishes and loaded with the complex dissolved in freshly prepared cell culture medium. They were incubated at 37 or 4 °C for the indicated time and washed at least 5–6 times with PBS before measurement. For the counter-staining experiment, cells were subsequently incubated at RT for 5 min with 100 μg mL^{-1} of acridine orange (from Invitrogen) and washed 10 times with PBS. Images were recorded with a Zeiss fluorescence microscope Axiovert S100 fitted with a Plan-Neofluar objective (20×), at λ_{exc} = 330 nm (BP = 80 nm) with an emission filter LP 585 nm for Eu^{III} and at λ_{exc} = 470 nm (BP 40 nm) with an emission filter BP 515–565 nm for acridine orange. Exposure times varied from 15 ms to 60 s.

Acknowledgements

This project is supported through a grant from the Swiss National Science Foundation. Selected funding by ESF-COST Action D38 is acknowledged. We thank Frédéric Gumy for his help in luminescence measurements and quantum yield determination, K. Lorentz for contributing to the synthesis of L^{C3}, Dr. A. Razaname for recording the ES-MS spectra of the complexes, and Dr. J. Raus from the Biomedical Research Institute "Dr. L. Willems-Instituut", University of Hasselt, Belgium, for kindly providing us with the hybridoma cell line 5D10.

[1] L. J. Martin, M. J. Hahnke, M. Nitz, J. Wohnert, N. R. Silvaggi, K. N. Allen, H. Schwalbe, B. Imperiali, *J. Am. Chem. Soc.* **2007**, *129*, 7106–7113.
[2] N. Johnsson, K. Johnsson, *ACS Chem. Biol.* **2007**, *2*, 31–38.
[3] J.-C. G. Bünzli, *Acc. Chem. Res.* **2006**, *39*, 53–61.
[4] J.-C. G. Bünzli, C. Piguet, *Chem. Soc. Rev.* **2005**, *34*, 1048–1077.
[5] S. Faulkner, S. J. A. Pope, B. P. Burton-Pye, *Appl. Spectrosc. Rev.* **2005**, *40*, 1–31.
[6] P. R. Selvin, *Annu. Rev. Biophys. Biomol. Struct.* **2002**, *31*, 275–302.
[7] K. Matsumoto, J. G. Yuan, *Lanthanide Chelates as Fluorescent Labels for Diagnostics and Biotechnology, Metal Ions in Biological Systems, Vol. 40* (Eds.: A. Sigel, H. Sigel), Marcel Dekker, New York, **2003**, Chapter 6.
[8] I. Hemmilä, V. M. Mukkala, *Crit. Rev. Clin. Lab. Sci.* **2001**, *38*, 441–519.
[9] W. L. Scaff, D. L. Dyer, K. Mori, *J. Bacteriol.* **1969**, *98*, 246–248.
[10] S. Phimphivong, S. S. Saavedra, *Bioconjugate Chem.* **1998**, *9*, 350–357.
[11] H. C. Manning, S. M. Smith, M. Sexton, S. Haviland, M. F. Bai, K. Cederquist, N. Stella, D. J. Bornhop, *Bioconjugate Chem.* **2006**, *17*, 735–740.
[12] H. C. Manning, T. Goebel, R. C. Thompson, R. R. Price, H. Lee, D. J. Bornhop, *Bioconjugate Chem.* **2004**, *15*, 1488–1495.
[13] M. P. Houlne, T. S. Agent, G. E. Kiefer, K. Mcmilian, D. J. Bornhop, *Appl. Spectrosc.* **1996**, *50*, 1221–1228.
[14] R. A. Poole, G. Bobba, M. J. Cann, J. C. Frias, D. Parker, R. D. Peacock, *Org. Biomol. Chem.* **2005**, *3*, 1013–1024.
[15] S. Pandya, J. H. Yu, D. Parker, *Dalton Trans.* **2006**, 2757–2766.
[16] R. Pal, D. Parker, *Chem. Commun.* **2007**, 474–476.
[17] K. Hanaoka, K. Kikuchi, H. Kojima, Y. Urano, T. Nagano, *J. Am. Chem. Soc.* **2004**, *126*, 12470–12476.
[18] B. Song, G. Wang, J. Yuan, *Chem. Commun.* **2005**, 3553–3555.
[19] J.-C. G. Bünzli, C. Piguet, *Chem. Rev.* **2002**, *102*, 1897–1928.
[20] C. Piguet, G. Bernardinelli, G. Hopfgartner, *Chem. Rev.* **1997**, *97*, 2005–2062.
[21] C. Piguet, M. Borkovec, J. Hamacek, K. Zeckert, *Coord. Chem. Rev.* **2005**, *249*, 705–729.
[22] S. Torelli, D. Imbert, M. Cantuel, G. Bernardinelli, S. Delahaye, A. Hauser, J.-C. G. Bünzli, C. Piguet, *Chem. Eur. J.* **2005**, *11*, 3228–3242.
[23] N. André, T. B. Jensen, R. Scopelliti, D. Imbert, M. Elhabiri, G. Hopfgartner, C. Piguet, J.-C. G. Bünzli, *Inorg. Chem.* **2004**, *43*, 515–529.
[24] T. B. Jensen, R. Scopelliti, J.-C. G. Bünzli, *Inorg. Chem.* **2006**, *45*, 7806–7814.
[25] T. B. Jensen, R. Scopelliti, J.-C. G. Bünzli, *Chem. Eur. J.*, DOI: 10.1002/chem.200700468.
[26] M. Elhabiri, R. Scopelliti, J.-C. G. Bünzli, C. Piguet, *J. Am. Chem. Soc.* **1999**, *121*, 10747–10762.
[27] C. D. B. Vandevyver, A.-S. Chauvin, S. Comby, J.-C. G. Bünzli, *Chem. Commun.* **2007**, 1716–1718.
[28] M. Elhabiri, J. Hamacek, J.-C. G. Bünzli, A.-M. Albrecht-Gary, *Eur. J. Inorg. Chem.* **2004**, 51–62.
[29] J.-C. G. Bünzli, in *Lanthanide Probes in Life, Chemical and Earth Sciences. Theory and Practice* (Eds.: J.-C. G. Bünzli, G. R. Choppin), Elsevier, Amsterdam, **1989**, Chapter 7, 219–293.
[30] K. Binnemans, C. Görller-Walrand, *Chem. Phys. Lett.* **1995**, *245*, 75–78.
[31] C. Görller-Walrand, K. Binnemans, *Rationalization of crystal field parameterization, Handbook on the Physics and Chemistry of Rare Earths, Vol. 23* (Eds.: K. A. Gschneidner, Jr., L. Eyring), Elsevier, Amsterdam, **1996**, Chapter 155.
[32] J.-C. G. Bünzli, B. Klein, D. Wessner, N. W. Alcock, *Inorg. Chim. Acta* **1982**, *59*, 269–274.

[33] S. T. Frey, W. D. Horrocks, Jr., *Inorg. Chim. Acta* **1995**, *229*, 383–390.
[34] C. Piguet, J.-C. G. Bünzli, G. Bernardinelli, G. Hopfgartner, S. Petoud, O. Schaad, *J. Am. Chem. Soc.* **1996**, *118*, 6681–6697.
[35] R. M. Supkowski, W. D. Horrocks, Jr., *Inorg. Chim. Acta* **2002**, *340*, 44–48.
[36] M. H. V. Werts, R. T. F. Jukes, J. W. Verhoeven, *Phys. Chem. Chem. Phys.* **2002**, *4*, 1542–1548.
[37] F. J. Steemers, W. Verboom, D. N. Reinhoudt, E. B. Vandertol, J. W. Verhoeven, *J. Am. Chem. Soc.* **1995**, *117*, 9408–9414.
[38] Z. Darzynkiewicz, *Methods Cell Biol.* **1990**, *33*, 285–298.
[39] A. B. Pangborn, M. A. Giardello, R. H. Grubbs, R. K. Rosen, F. J. Timmers, *Organometallics* **1996**, *15*, 1518–1520.
[40] J.-C. G. Bünzli, C. Mabillard, *Inorg. Chem.* **1986**, *25*, 2750–2754.
[41] G. Schwarzenbach, *Complexometric Titrations*, Chapman and Hall, London, **1957**.
[42] C. Piguet, G. Bernardinelli, B. Bocquet, A. Quattropani, A. F. Williams, *J. Am. Chem. Soc.* **1992**, *114*, 7440–7451.
[43] G. Black, E. Depp, B. B. Corson, *J. Org. Chem.* **1949**, *14*, 14–21.
[44] K. N. Raymond, *Chem. Eng. News* **1983**, *61*, 4–4.
[45] E. R. Malinowski, D. G. Howery, *Factor Analysis in Chemistry*, Wiley, New York, **1991**.
[46] H. Gampp, M. Maeder, C. J. Meyer, A. D. Zuberbühler, *Talanta* **1985**, *32*, 257–264.
[47] H. Gampp, M. Maeder, C. J. Meyer, A. D. Zuberbühler, *Talanta* **1986**, *33*, 943–951.
[48] A.-S. Chauvin, F. Gumy, D. Imbert, J.-C. G. Bünzli, *Spectrosc. Lett.* **2004**, *37*, 517–532; erratum: A.-S. Chauvin, F. Gumy, D. Imbert, J.-C. G. Bünzli, *Spectrosc. Lett.* **2006**, *40*, 193.
[49] B. Fanget, O. Devos, M. Draye, *Anal. Chem.* **2003**, *75*, 2790–2795.
[50] J. C. de Mello, H. F. Wittmann, R. H. Friend, *Adv. Mater.* **1997**, *9*, 230–232.
[51] F. Gumy, J.-C. G. Bünzli, unpublished work, **2006**.
[52] R. Rodriguez-Cortinas, F. Avecilla, C. Platas-Iglesias, D. Imbert, J.-C. G. Bünzli, A. de Blas, T. Rodriguez-Blas, *Inorg. Chem.* **2002**, *41*, 5336–5349.
[53] M. Ishiyama, M. Shiga, K. Sasamoto, M. Mizoguchi, P. G. He, *Chem. Pharm. Bull.* **1993**, *41*, 1118–1122.
[54] M. Ishiyama, K. Sasamoto, M. Shiga, Y. Ohkura, K. Ueno, K. Nishiyama, I. Taniguchi, *Analyst* **1995**, *120*, 113–116.
[55] C. Korzeniewski, D. M. Callewaert, *J. Immunol. Methods* **1983**, *64*, 313–320.
[56] T. Decker, M. L. Lohmannmatthes, *J. Immunol. Methods* **1988**, *115*, 61–69.

Received: June 11, 2007
Published online: September 18, 2007

